Bond-Slip Behaviour of Deformed Bars Embedded In Engineered Cementitious Composites: Experimental and Analytical Investigation

M. Sravanthi
Assistant Professor
Department of Civil Engineering
St Martin's Engineering College
Corresponding Author's Email: *msravanthice@smec.ac.in*

Abstract

This paper investigates the bond-slip behaviour of steel reinforcement embedded in engineered cementitious composites (ECC), a ductile concrete exhibiting tensile strain hardening performance. Two series of experimental tests were carried out on short and long reinforcement subject to pull-out actions. The maximum bond stress that embedded steel reinforcement could sustain was quantified through pullout tests on short rebars. Experimental results of short reinforcement suggested that ECC significantly increased the maximum bond stress of steel reinforcement. For long reinforcement, special attention was paid to the bond stress of steel segments at post-yield stage. Bond stress profiles were determined in accordance with attached strain gauge measurements along the steel bars. Besides, the effect of localised necking beyond ultimate strength on the force-slip relationships of reinforcement was studied. Thereafter, an analytical model was proposed based on experimental results to predict the force-slip relationship of long reinforcement either anchored in concrete or in ECC. Reasonably good agreement was achieved between experimental and analytical force-slip curves. Finally, parametric studies were conducted to quantify the required embedment length of steel reinforcement in ECC.

Keywords*-: bond-slip behavior, ECC significantly, analytical force-slip curves.*

 Page 128-141 © MANTECH PUBLICATIONS 2023. All Rights Reserved

INTRODUCTION

Engineered cementitious composites (ECC) display superior strain-hardening behaviour and ultra-high strain capacity in uniaxial tension compared to normal concretes [1]. By tailoring the fibre, cement matrix, and fibre-matrix interface properties based on the micro-mechanical model, a tensile strain capacity of up to 5% can be achieved under static and impact loading conditions [2]. Experimental tests on reinforced ECC beams and columns showed that ECC could significantly enhance structural resistance and energy absorption capacity under earthquake-induced cyclic loadings [3,4]. When it was used in beam-column connections without transverse steel reinforcement, ECC exhibited superior damage tolerance and sustained substantial shear distortions under cyclic loads [5]. Besides, ECC could improve bond efficiency of reinforcement by reducing slippage of column bars [6]. Therefore, ECC is recommended by the Japan Society of Civil Engineers for potential applications in structural members [7], in which the tensile strength of ECC can be considered in design practice. In addition to strain-hardening behaviour of ECC under uniaxial tension, the interactions between steel reinforcement and ECC play a significant role in enhancing the energy dissipation of reinforced ECC members. Compatible deformations between steel reinforce ment and ECC were observed at multiple cracking stage [8,9]. However, beyond the tensile strain capacity of ECC, severe localisation of major cracks was reported due to tension stiffening behaviour of reinforced ECC members [10–12]. Thus, bond stress of reinforcement embedded in ECC has to be quantified through experimental tests. Currently available test data mainly focus on bond-slip models of longitudinal reinforcement in flexural members such as beams [13–15]. In these cases, longitudinal splitting cracks could propagate along embedded reinforcing bars due to either inadequate concrete cover or close bar spacing.

When the bond-slip model is used for longitudinal reinforcement in beam-column joints, significant underestimation of bond stress can be expected, as reinforcement in the joint is generally well-confined by thick concrete cover or closely spaced stirrups. Therefore, it is necessary to investigate the bond-slip behaviour of steel reinforcement embedded in beam-column joints. This paper presents an experimental investigation on the bondslip behaviour of reinforcement embedded in ECC. Two series of pull-out tests were conducted on short and long embedded reinforcement. The objectives were twofold, viz. (a) to evaluate the effect of concrete or ECC on bond stress of short reinforcement and (b) to calculate the bond stress along each steel segment of long reinforcement based on strain gauge measurements. From

Page 128-141 © MANTECH PUBLICATIONS 2023. All Rights Reserved

(a) and (b), one can gain physical insights into the interactions between either short or long reinforcement with ECC. Furthermore, an analytical model was proposed for evaluating the bond-slip relationship of embedded reinforcement in ECC and validated through experimental results. Design recommendations were made for steel reinforcement embedded in ECC based on experimental and analytical results.

Experimental programme

Specimen design In the experimental programme, two series of experimental tests were conducted on reinforcement embedded in either conventional concrete or ECC. Table 1 summarises the details of steel reinforcement. In the first series, six steel bars with 13 mm diameter were pulled out from reinforced concrete and ECC blocks and their embedment length was only 65 mm (five times the rebar diameter), as shown in Fig. 1(a). Thus, similar to the pull-out tests by Eligehausen et al. [16], local bond-slip behaviour of short reinforcement was investigated at the elastic stage only. By increasing the embedment length, steel reinforcement may develop inelastic behaviour before failure occurs. After yielding of reinforcement, bond stress along the yielded steel segments reduces significantly due to inelastic elongation of reinforcement and shearing-off of concrete keys between steel lugs [17,18]. Therefore, post-yield bond stress of long reinforcement has to be studied as well.

JSCE [7] suggested that the minimum embedment length of reinforcement in ECC can be taken as twenty times the rebar diameter. Accordingly, to study the post-yield bond stress of reinforcement, steel bars of 13 mm nominal diameter were tested in the second series, and their embedment length was increased to 260 mm (see Fig. 1(a)). Twelve specimens were designed in total, out of which six were embedded in conventional concrete and the other six in ECC. It is noteworthy that two 4.5 mm wide and 2.5 mm deep grooves were cut along the longitudinal ribs, as shown in Fig. 1(a). Post-yield strain gauges with 2 mm gauge length were mounted along the grooves on both sides of the reinforcement at intervals of 32.5 mm in the middle segment and 27.5 mm at the two end segments (see Fig. 1(b)). Under pull-out loads, local failure cone of concrete would form at the active end of embedded reinforcement [19,20], which would lead to bond deterioration and reduce the embedment length of reinforcement. The depth of the failure cone is generally around five times the diameter of reinforcement [21]. Therefore, to prevent the formation of failure cone of concrete, PVC pipes with 20 mm diameter and 65 mm length were provided at each end of short and long

Page 128-141 © MANTECH PUBLICATIONS 2023. All Rights Reserved

reinforcement and the effective embedment lengths of short and long reinforcement were kept as 65 mm (5/) and 260 mm (20/), respectively, as shown in Fig. 1(a). Four deformed longitudinal bars of 10 mm diameter, along with transverse reinforcement of 6 mm diameter at 100 mm centre-to-centre spacing, were placed in the concrete block to avoid potential failure. 2.2. Test set-up and instrumentation Fig. 2 shows the test set-up for reinforcement under pull-out forces.

Four PVC pipes were embedded in concrete blocks, through which four steel bolts were placed to connect the top and the bottom steel plates together. On top of the steel plate, a circular opening with a diameter of 80 mm (see Fig. 2(a)) was cut to reduce the effect of compression force on the bond stress of reinforcement. A similar opening was also made in the bottom plate to facilitate measurement of slip at the free end of reinforcement. Projected steel reinforcement from the concrete block through the bottom plate was clamped by the testing machine to apply pull-out force to the embedded reinforcement. Applied load and axial displacements were directly measured by the testing machine. Besides, linear variable differential transducers (LVDTs) were installed at the loaded and free ends of the reinforcement to measure the slip of reinforcement relative to the concrete block, as shown in Fig. 2 (a) and (b). For long reinforcement with an effective embedment length of 260 mm, strain gauges were used to monitor the variations of steel strains along the embedment length (see Fig. 1(b)). 3. Test results and discussion 3.1. Material properties Material tests were carried out on steel reinforcement H13 and ready mix concrete grade 30. Table 2 summarises the material and geometric properties of original and grooved reinforcement. Fig. 3 (a) shows a typical stress-strain curve of reinforcement in tension. Average compressive strength for three samples of 150 mm diameter by 300 mm long concrete cylinders was determined as 31.8 MPa. ECC was prepared by mixing water, ordinary Portland cement, ground granulated blast-furnace slag (GGBS), silica sand, superplasticizer, and micro-polyvinyl alcohol (PVA) fibres. Table 3 gives the mix proportions of ECC. The water-binder ratio of ECC was 0.27 and 60% of binder was replaced by GGBS. The volume fraction of PVA fibres with 39 lm in diameter and 12 mm in length was 2%. Material properties of ECC were also obtained by means of compression and uniaxial tension tests. The average compressive strength for three samples of 50 mm diameter by 100 mm long ECC cylinders was 53.2 MPa. When subjected to uniaxial tension, ECC dogbone specimens with a cross section of 10.5 mm thickness by 36 mm width and a gauge length of 150 mm exhibited significant strain-hardening behaviour, as

Page 128-141 © MANTECH PUBLICATIONS 2023. All Rights Reserved

shown in Fig. 3(b). The first cracking strength of ECC was 3.2 MPa. Thereafter, multiple fine cracks developed along the gauge length perpendicular to the loading axis, leading to several drops of the load prior to failure. The ultimate tensile strain capacity was around 1.2%.

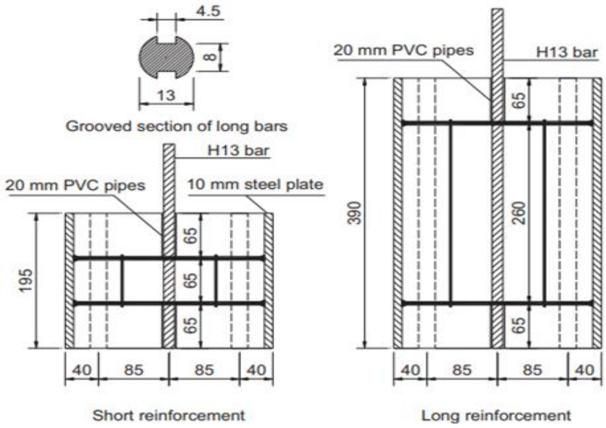

Details of Specimens

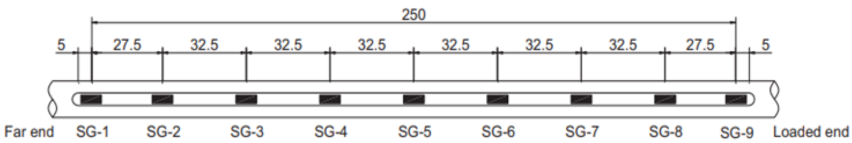

Layout of strain gauges along long a reinforcing bar

Bond strength of short reinforcement

In the experimental tests, applied force and associated slip of short reinforcement were measured at the loaded end. By assuming constant bond stress distribution along the embedment length, bond stress at each load level was calculated by the applied load divided by the contact area of steel reinforcement and surrounding concrete or ECC. Fig. 4 shows the bond stress-slip curves of short reinforcement under pull-out forces. At the initial stage, bond stress increased with slip of reinforcement at the loaded end. Nearly the same maximum bond stresses were obtained in the experimental tests of short bars embedded in conventional concrete, as shown in Fig. 4(a). The average bond stress of three specimens was obtained as 17.1 MPa. However, the maximum force sustained by the steel reinforcement was much lower than the yield force, indicating that reinforcement remained at its elastic stage. Beyond the maximum bond stress, bond stress decreased with increasing slip at the loaded end and short steel reinforcement was pulled out from surrounding concrete as a result of insufficient embedment length. Similar bond-slip curves were also obtained for reinforcement embedded in ECC. However, ECC substantially increased the maximum bond stress on reinforcement

Page 128-141 © MANTECH PUBLICATIONS 2023. All Rights Reserved

compared to concrete, as shown in Fig. 4(b). The mean value for three specimens (with 5dia anchorage length) was quantified as 24.9 MPa, nearly 45% greater than that of reinforcement in concrete. Higher bond stress between steel reinforcement and ECC resulted from the strain-hardening behaviour of ECC. After the formation of radial cracks around the reinforcement, ECC is able to carry the load continuously and to provide lateral confinement to the steel reinforcement. Thus, the peak bond stress in ECC was substantially increased compared to concrete specimens. To consider the effect of compressive strength of specimens, the maximum bond stress was normalised by 0 c q , where f 0 c is the compressive strength of concrete or ECC cylinders. Thus, the values could be determined as 3:0$\sqrt{f'_{c'}}$ c q and 3:4 $\sqrt{f'_{c'}}$ 0 c q for reinforcement embedded in concrete and ECC, respectively.

Compared to conventional concrete, ECC provided around 14% greater bond stress for short reinforcement. Besides, bond stress obtained from pull-out tests on short reinforcement embedded in concrete was significantly greater than that given by Bandelt and Billington [13] and Eligehausen et al. [16], possibly due to adequate concrete cover so that splitting cracks were prevented on the surface of the concrete block.

Bond-slip behaviour of long reinforcement

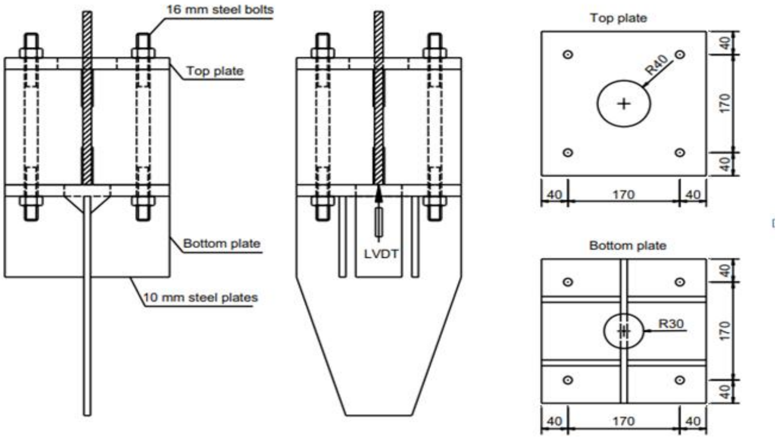

Schematic view (all units are in mm)

3.3.1. Force-slip curves When the embedment length of reinforcement was increased to 260 mm (20/), significantly different bond-slip behaviour was observed from that of short reinforcement. Fig. 5(a) and (b) shows the force-slip relationships of long reinforcement. All the steel bars could develop their ultimate strength. Beyond the yield capacity of steel bars,

 Page 128-141 © MANTECH PUBLICATIONS 2023. All Rights Reserved

long reinforcement experienced softening and eventually fractured at the onset of grooved sections (see Fig. 6(a)), instead of pull-out failure at elastic stage for short reinforcement. The surrounding ECC matrix remained intact during the whole pull out process, as shown in Fig. 6(b). Table 4 summarises the critical loads and corresponding slips at the loaded end of long reinforcement. Compared to conventional concrete, long reinforcement embedded in ECC developed nearly the same yield, ultimate and rupture forces, as shown in Table 4.

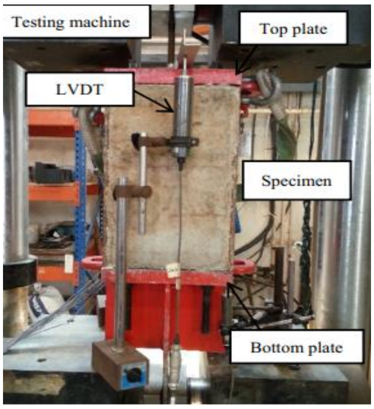

Test set-up Set-up for pull-out tests

Table 2

Material and geometric properties of steel reinforcement.

Steel bars	Elastic modulus (GPa)	Yield strength (MPa)	Hardening modulus (MPa)	Ultimate strength (MPa)	Softening modulus (GPa)	Rupture stress (MPa)
H13	191.8	561	1232	658	14.5	456
	Effective circumference of grooved bars (mm)	Net area of grooved bars (mm^2)	Circumference of original bars (mm)		Area of original bars (mm^2)	
	31.0	105.9	42.0		127.8	
	Lug spacing (mm)		Lug inclination (°)		Lug area (mm^2)	
	9		62.0		13.9	

Table 3

Mix proportions of ECC.

Ingredient	Cement	GGBS	Water	Silica sand	PVA fibre
Unit weight (kg/m^3)	574	860	387	287	26

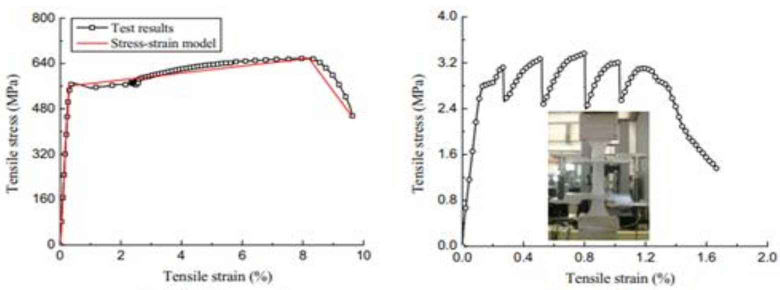

(a) Reinforcement (b) ECC

Stress –Strain curves of steel reinforcement and ECC

Page 128-141 © MANTECH PUBLICATIONS 2023. All Rights Reserved

International Journal of Advance Civil Engineering and Technology
Volume 8, Issue 2, July-December, 2023

Besides, slip at the free end of long reinforcement was also measured through LVDT (see Fig. 2(a)). Fig. 5(c) and (d) shows the applied load versus free-end-slip curves of long reinforcement. It was observed that slip at the free end increased with applied load and attained its maximum value at the ultimate load capacity of reinforcement. The average values of maximum slips at the free end were around 0.75 mm in concrete and 0.69 mm in ECC. Thereafter, a reduction in applied load due to necking of steel bars gradually reduced the free end slip until fracture of reinforcement occurred near the loaded end. Test results indicate that the embedment length of steel reinforcement (20/) is inadequate to ensure zero free end slip.

Table 4

Slips of reinforcement at critical loads.

Specimen	Yield force F_y (kN)	Slip at F_y (mm)	Ultimate force F_u (kN)	Slip at F_u (mm)	Rupture force F_r (kN)	Slip at F_r (mm)
LC-1	65.6	1.44	75.8	5.77	57.2	10.14
LC-2	59.7	1.67	71.0	7.16	51.6	13.06
LC-3	61.7	1.21	73.4	5.27	52.7	11.78
LC-4	64.9	1.25	74.2	7.35	51.6	12.61
LC-5	61.8	1.15	73.8	4.53	50.2	10.02
LC-6	64.6	1.54	74.3	4.79	52.5	10.28
Mean value	63.1	1.38	73.8	5.81	52.6	11.32
Coefficient of variation	3.4%	13.6%	1.9%	18.8%	4.2%	10.9%
LE-1	62.5	0.95	74.4	3.64	49.6	9.55
LE-2	64.0	1.13	75.7	4.37	55.8	9.59
LE-3	58.4	0.91	71.9	3.88	54.1	8.39
LE-4	60.6	1.31	71.0	4.64	45.8	9.68
LE-5	60.3	1.11	71.1	3.89	46.5	8.99
LE-6	68.2	1.34	79.3	4.53	56.3	9.56
Mean value	62.3	1.13	73.9	4.16	51.4	9.29
Coefficient of variation	5.1%	14.4%	4.0%	9.0%	8.3%	4.9%

Note: the elongation of reinforcement at the unbonded region was deducted from the measured slip at the loaded end by calculating the strain of reinforcement at the loaded end and assuming that it was constant at the unbonded region.

3.3.2. Steel strain profiles In addition to measured forces and slips of reinforcement, steel strains at specific sections were recorded by strain gauges, as shown in Fig. 1(b). Fig. 7(a) and (b) shows the steel strain profiles along the embedment length of long reinforcement in ECC. At elastic stage, only limited embedment length of reinforcement was mobilised to transfer bond stress to surrounding concrete, as shown in Fig. 7(a). When the yield strength was attained at the loaded end, nearly the full length of embedded reinforcement sustained tensile strain, with zero strain at the free end and the maximum strain at the loaded end.

Furthermore, after the onset of inelastic behaviour at the loaded end, strains of yielded steel segments near the loaded end were several times greater than that of elastic segments, as shown in Fig. 7(b). At the load capacity of long reinforcement, total length of inelastic steel segments was around 60 mm, and the remaining steel segments were at elastic stage. Thereafter the length of elastic steel segments remained nearly the same as that at the ultimate load of steel reinforcement. However, strains of inelastic steel segments were substantially increased due to localised elongation of reinforcement before fracture. 3.3.3.

Page 128-141 © MANTECH PUBLICATIONS 2023. All Rights Reserved

Bond stress profiles With measured steel strains along the embedment length of long reinforcement, bond stress over each steel segment can be 4. Analytical bond-slip model An analytical bond-slip model is proposed for reinforcement embedded in concrete and ECC in accordance with the experimental results. In the model, bond stress of reinforcement is related to slip at the loaded end if steel reinforcement exhibits elastic behaviour under pull-out forces. Once plasticity kicks in near the loaded end, post-yield bond stress calculated from long reinforcement can be utilised. Besides, by defining the trilinear stress-strain model for steel reinforcement (see Fig. 3(a)), an attempt is made to study the bond-slip behaviour of reinforcement at softening stage due to necking of reinforcement near the loaded end. 4.1.

Bond-slip model At the elastic stage of steel reinforcement, bond-slip models proposed by Eligehausen et al. [16] and Chao et al. [22] are modified according to test results, as expressed in Eq. (2). The maximum bond stress is quantified through pull-out tests on short reinforcement embedded in concrete and ECC. As a result of better confinement provided by concrete and ECC, slip of reinforcement at the onset of maximum bond stress was increased to 1.5 mm. The frictional bond stress is assumed to be 37% of the maximum bond stress, as reported by Eligehausen et al. [16] for short reinforcement embedded in concrete. Table 5 includes the bond stress and slip of reinforcement anchored in concrete and ECC. The modified model agrees reasonably well with the bond-slip relationships of short reinforcement embedded in conventional concrete and ECC, as shown in Fig. 4(a) and (b). where s1 is the maximum bond stress of reinforcement; s1 is the slip at the onset of maximum bond stress; s2 is the slip at the end of maximum bond stress; s2 is the frictional bond stress; and s3 is the slip at the onset of frictional bond. Long reinforcement anchored in ECC developed inelastic behaviour close to the loaded end, as shown in Fig. 7(b). Thus, it is necessary to evaluate the bond stress at the post-yield stage of reinforcement. In the experimental tests, average post-yield bond stresses were determined as 4.2 MPa (around 0:75 f 0 c q) and 5.7 MPa (around 0:78 0 c q) for reinforcement in concrete and ECC, respectively. Besides, the post-yield bond stress can also be calculated from the frictional bond, if Poisson effect caused by contraction of cross section at the inelastic stage of reinforcement can be appropriately considered [23]. It is reported that Poisson effect reduces the bond stress by 20–30% [16]. As a result, a reduction factor of 70% can be selected to quantify the post-yield bond stress from the frictional bond. Hence, corresponding values are determined as 0:8 c q and 0:9 0 c q for reinforcement anchored in concrete and ECC,

 Page 128-141 © MANTECH PUBLICATIONS 2023. All Rights Reserved

respectively. These values are close to the experimental results of long reinforcement. 4.2. Calibration of analytical model A nested iteration procedure is developed to estimate the force slip relationship of long reinforcement. In the procedure, the embedded reinforcement is discredited into steel segments with a length of one rebar diameter. For each steel segment, relative slip at the two ends has to be assumed. Besides, it is further assumed that bond stress is constant along the steel segment, as shown in Fig. 8(a). Correspondingly, bond stress can be calculated from the average slip at the centre of the segment in accordance with the proposed bond-slip model, and then total bond force acting on the segment can be computed, as expressed in Eq. (3). It is noteworthy that the steel force at the free end of reinforcement is zero. Hence, from the free end onwards, equilibrium of each steel segment can be established and steel strain at each section can be determined from the stress-strain model of reinforcement, as given by Eq. (1). Furthermore, compatibility of slips at both ends of the segment has to be satisfied (see Fig. 8(b)). Thus, slips at the ends of the steel segment can be calculated through Eq. (4). DF ¼ sp/Dl ð3Þ s2 ¼ s1 þ 1 2 ðe1 þ e2ÞDl ð4Þ where DF is the difference between forces at two ends of a steel segment; s is the bond stress along a steel segment; / is the diameter of a reinforcement; Dl is the length of a steel segment; e1 and e2 are the steel strains at both ends of a steel segment; s1 and s2 are associated slips. In accordance with the proposed analytical model and bond stresses obtained from the experimental tests, the force-slip relationships of embedded steel reinforcement can be predicted. Fig. 9 shows the analytical force-slip curves of long reinforcement in concrete and ECC. Comparisons between experimental and analytical results indicate that the analytical force-slip curves of reinforcement agree well with experimental results. Apparently, three stages can be categorised in the force-slip curves, namely, elastic ascending, hardening and post-peak softening stages.

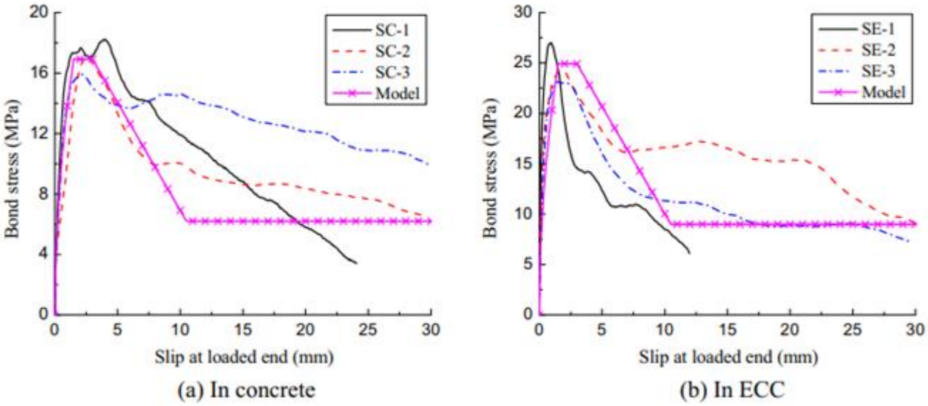

Force-slip relationships of short reinforecement

Page 128-141 © MANTECH PUBLICATIONS 2023. All Rights Reserved

However, previous analytical studies on the bond-slip behaviour of reinforcement only focused on the elastic ascending and hardening stages, with little attention paid to the post-peak softening stage due to necking of steel reinforcement [24,25]. Therefore, the ultimate slip of reinforcement was considerably underestimated, in particular, under large deformation state in which fracture of reinforcement may eventually occur.

Parametric study Based on the proposed analytical bond-slip model in Section
4.2, a parametric study is conducted on the effect of embedment length on force-slip relationships of embedded reinforcement in concrete and ECC. In the study, four modes of failure, namely, elastic pullout, post-yield pull-out, fracture with and without free end slip, are defined for steel reinforcement with various embedment lengths, as included in Table 6. Corresponding embedment lengths are calculated through the proposed model. When the ratio of the embedment length to diameter of steel bars embedded in ECC is less than 8, reinforcement exhibits pullout failure at elastic stage, similar to that observed in pull-out tests of short reinforcement. When the ratio is in the range of 8–12, reinforcement develops inelastic behaviour at the loaded end, but is eventually pulled out from surrounding ECC. By increasing the ratio beyond 12, fracture of reinforcement occurs at the loaded end. However, slip at the free end of reinforcement can still be mobilised due to insufficient embedment length, as discussed in pull-out tests of long reinforcement. A further increase in the ratio does not alter the failure mode of reinforcement, whereas slip at the free end of reinforcement is gradually reduced, leading to reduction in associated bond stress. The ratio has to be greater than 30 in order to fully eliminate the free end slip. Compared to ECC, the required embedment lengths of reinforcement in concrete have to be increased to 35 times its diameter, as shown in Table 6. Therefore, ECC can reduce the embedment length of steel reinforcement by 14% if free end slip is prevented. It is noteworthy that the embedment length of steel reinforcement in ECC and concrete is determined for a compressive strength of 31.8 MPa. By increasing the compressive strength, the required embedment length is apparently reduced. If the actual compressive strength of ECC is 53.2 MPa, the required embedment lengths become 10 and 26 times rebar diameter for fracture of steel reinforcement with and without free end slip, respectively. Therefore, compared to conventional concrete, the embedment length of steel reinforcement in ECC can be substantially reduced. Fig. 10 shows the load-slip curves of steel reinforcement embedded in ECC.

 Page 128-141 © MANTECH PUBLICATIONS 2023. All Rights Reserved

Discussions

JSCE [7] specifies the basic embedment length of reinforcement in ECC, in which bond stress of steel bars is assumed to be identical to that in concrete. If safety factor is not considered, the required embedment length of steel bar H13 can be determined as 26/ so as to develop its yield strength. Analytical results also show that steel reinforcement with such an embedment length can develop its ultimate tensile strength without slip at the free end when the compressive strength of ECC is 53.2 MPa. Thus, design values for embedment length of reinforcement are quite conservative compared to analytical results. Additionally, test results of long reinforcement in ECC indicate that steel bars with shorter embedment length could develop their ultimate strength, even though slip and bond stress at the free end of reinforcement were mobilised to resist the applied load. Analytical bond-slip model predicts the minimum embedment length of reinforcement as 10/. However, slip at the free end is undesirable for embedded reinforcement, as it increases the total slip of reinforcement and reduces the energy dissipation capacity, in particular under cyclic loading conditions. Therefore, the embedment length of reinforcement in ECC needs to be at least 26/ so as to prevent slip at the free end. Moreover, the value should be further increased when the confinement condition of reinforcement is less than that in the experimental tests.

CONCLUSIONS

In this paper, bond-slip behaviour of short and long steel reinforcement embedded in well-confined conventional concrete and ECC was investigated experimentally. Short reinforcement with embedment length of five times rebar diameter exhibited pull-
Acknowledgement The authors would like to acknowledge the financial support from Protective Technology Research Centre in Nanyang Technological University, Singapore. Special thanks are extended to Universiti Teknologi MARA, Malaysia, for its research scholarship.

REFERENCES

1. V.C. Li, On engineered cementitious composites (ECC)-a review of the material and its applications, J. Adv. Concr. Technol. 1 (3) (2003) 215–230.
2. E. Yang, V.C. Li, Tailoring engineered cementitious composites for impact resistance, Cem. Concr. Res. 42 (8) (2012) 1066–1071.

 © MANTECH PUBLICATIONS 2023. All Rights Reserved

3. G. Fischer, V.C. Li, Deformation behavior of fiber-reinforced polymer reinforced engineered cementitious composites (ECC) flexural members under reversed cyclic loading conditions, ACI Struct. J. 100 (1) (2003) 25–35.
4. H. Fukuyama, Y. Sato, V.C. Li, Y. Matsuzaki, H. Mihashi, Ductile engineered cementitious composite elements for seismic structural application, in: Proceedings of the 12th World Conference on Earthquake Engineering, New Zealand, 2000.
5. G.J. Parra-Montesinos, High-performance fiber-reinforced cement composites: an alternative for seismic design of structures, ACI Struct. J. 102 (5) (2005) 668–675.
6. G.J. Parra-Montesinos, J.K. Wight, Seismic response of exterior RC column-tosteel beam connections, J. Struct. Eng. 126 (10) (2000) 1113–1121.
7. JSCE, Recommendations for design and construction of high performance fiber reinforced cement composites with multiple fine cracks (HPFRCC), Concrete Engineering Series 82, Japan Society of Civil Engineers, 2008.
8. G. Fischer, V.C. Li, Effect of matrix ductility on deformation capacity behavior of steel-reinforced ECC flexural members under reversed cyclic loading conditions, ACI Struct. J. 99 (6) (2002) 781–790.
9. V.C. Li, G. Fischer, Reinforced ECC-an evolution from materials to structures, in: Proceedings of the 1st fib Congress, Osaka, Japan, 2002.
10. D.M. Moreno, W. Trono, G. Jen, C. Ostertag, S. Billington, Tension stiffening in reinforced high performance fiber reinforced cement-based composites, Cem. Concr. Compos. 50 (2014) 36–46.
11. S.-B. Kang, K.H. Tan, E.-H. Yang, Progressive collapse resistance of precast beam-column sub-assemblages with engineered cementitious composites, Eng. Struct. 98 (2015) 186–200.
12. D.M. Moreno, W. Trono, G. Jen, C. Ostertag, S.L. Billington, Tension stiffening in reinforced high performance fiber reinforced cement-based composites under direct tension, High Perform. Fiber Reinf. Cem. Compos. 6 (2) (2012) 263–270.
13. M.J. Bandelt, S.L. Billington, Bond behaviour of steel reinforcement in highperformance fiber-reinforced cementitious composite flexural members, Mater. Struct. 49 (1) (2016) 71–86.
14. T. Kanakubo, H. Hosoya, Bond-splitting strength of reinforced strain-hardening cement composite elements with small bar spacing, ACI Struct. J. 112 (2) (2015) 189–198.

 © MANTECH PUBLICATIONS 2023. All Rights Reserved

15. K. Asano, T. Kanakubo, Study on size effect in bond splitting behavior of ECC, High Perform. Fiber Reinf. Cem. Compos. 6 (2) (2012) 137–144.
16. R. Eligehausen, E.P. Popov, V.V. Betero, Local Bond Stress-Slip Relationships of Deformed Bars under Generalized Excitations Report No. UCB/EERC-83/23, College of Engineering, University of California, Berkeley, 1983.
17. A.J. Bigaj, Bond Behaviour of Deformed Bars in NSC and HSC-Experimental Study Report No. 25.5-95-11, Steven Laboratory, Faculty of Civil Engineering, Delft University of Technology, 1995.
18. H. Shima, L.L. Chou, H. Okamura, Micro and macro model for bond in reinforced concrete, J. Fac. Eng., Univ. Tokyo (B) 39 (2) (1987) 133–194.
19. B. Engström, J. Magnusson, Z. Huang, Pull-out bond behavior of ribbed bars in normal and high-strength concrete with various confinements, ACI Spec. Publ. 180 (1998) 215–242.
20. S. Viwathanatepa, E.P. Popov, V.V. Bertero, Effects of Generalized Loadings on Bond of Reinforcing Bars Embedded in Confined Concrete Blocks, Report No. UCB/EERC-79/22, College of Engineering, University of California, Berkeley, 1979.
21. M. Soltani, K. Maekawa, Path-dependent mechanical model for deformed reinforcing bars at RC interface under coupled cyclic shear and pullout tension, Eng. Struct. 30 (4) (2008) 1079–1091.
22. S.-H. Chao, A.E. Naaman, G.J. Parra-Montesinos, Local bond stress-slip models for reinforcing bars and prestressing strands in high-performance fiberreinforced cement composites, ACI Spec. Publ. 272 (2010) 151–172.
23. S. Pochanart, T. Harmon, Bond-slip model for generalized excitations including fatigue, ACI Mater. J. 86 (5) (1989) 465–474.
24. J. Yu, K.H. Tan, Macromodel-based simulation of catenary action of RC beamcolumn sub-assemblages, in: Proceedings of the 3rd Fib International Congress 2010, Washington, DC, 2010.
25. L.N. Lowes, N. Mitra, A. Altoontash, A beam-column joint model for simulating the earthquake response of reinforced concrete frames, PEER Report 2003/10, Pacific Earthquake Engineering Research Center, University of California, Berkeley, 2004.

Page 128-141 © MANTECH PUBLICATIONS 2023. All Rights Reserved